Kinetic study of combustion behavior in a gas turbine -Influence from varying natural gas composition

Catharina Tillmark

April 18, 2006

Lund University
Dept. of Energy Sciences
P.O.Box 118, SE-221 00 Lund

ISRN LUTMDN/TMHP–06/5093–SE
ISSN 0282-1990

Abstract

The purpose of the numerical study was to investigate the influence of three different natural gas compositions on the combustion behaviour of an Advanced Environmental Vortex (AEV) burner. The flow conditions apply to the AEV burners installed in the Siemens gas turbine SGT-800.

Numerical simulations were carried out using the software Chemkin 4. Ignition temperatures, adiabatic flame temperatures, NO_X emissions and laminar flame speeds were determined using models included in the software.

To find suitable reaction mechanisms for the simulations a mechanism study was made. The behaviour of the mechanisms was studied burning methane and ethane. The two reaction mechanisms chosen for the simulations represent combustion of hydrocarbons with up to two carbon atoms and seven carbon atoms. The reaction mechanisms are developed by Danmarks tekniske universitet and Lawrence Livermore National Laboratory respectively.

The simulations gave the following results. The ignition temperature differed up to 80 K and the adiabatic flame temperature up to 30 K between the gases. The highest NO_X emissions were obtained at Φ=0.95 and increased with the residence time. The largest difference in laminar flame speed was 10 cm/s.

The conclusion from the results when applied to the conditions in the AEV burner is that the difference in gas composition does not influence the performance of the burner noticeably. However some differences in NO_X emissions are noticed but since NO_X emissions are difficult to predict the levels of the emissions are to be treated with caution.

Contents

List of Figures

List of Tables

1 Nomenclature

a_e	Surface area per unit length	[m]
A_i	Frequency factor	[various]
c_p	Specific heat at constant pressure	[J/kg-K]
D	Mass diffusion coefficient	[m^2/s]
E_i	Activation energy	[J/mole]
F	Friction force	[N]
h_k	Specific enthalpy	[J/g]
I	Total number of reactions	[-]
k	Thermal conductivity	[W/mK]
k_f	Forward rate coefficient	[various]
k_G	Global rate coefficient	[various]
k_r	Reversed rate coefficient	[various]
K	Total number of species	[-]
K_{ci}	Equlibrium constant in concentration units	[-]
Le	Lewis number	α/D
$\dot{m}$	Mass flow	[g/s]
n	Number of molecules	[-]
p	Pressure	[Pa]
q_i	Rate of progress variable	[mole/m^2s]
Q	Energy flux	[J/s]
R	Specific gas constant	[J/kg-K]
R_c	Universal gas constant	[J/moleK]
t	Time	[s]
T	Temperature	[K]
u	Axial velocity	[m/s]
U_{sys}	Inner energy of a closed system	[J]
V	Volume	[m^3]
W	Molecular weight	[g/mol]
x	Distance	[m]
$[X]$	Molar concentration	[mole/m^3]
Y	Mass fraction	[-]

Greek symbols

α	Thermal diffusivity	[m^2/s]
β_i	Temperature exponent	[-]
ρ	Density	[g/m^3]
τ	Residence time	[s]
υ_{ki}	Net stoichiometric coefficient	[-]
υ'_{ki}	Stoichiometric coefficient reactant species	[-]
υ''_{ki}	Stoichiometric coefficient product species	[-]
$\dot{\omega}_k$	Species production rate	[mole/cm^3s]

Subscript

f	Forward
i	ith reaction
k	kth species
r	Reverse

2 Introduction

One of the most common fuels in gas turbines used for power generation is natural gas. Since natural gas consists of many species the composition of the gas varies. The variation of the natural gas depends both on origin and treatment. For instance the higher hydrocarbons and carbon oxides are removed from the gas when chilled to LNG due to safety reasons.

The gas turbine SGT−800 from Siemens AG has been delivered to sites around the world with various compositions of natural gas. The affect the composition variations, considered proportionately small, have on the combustion is not well known. The question arised if the difference in natural gas composition makes a difference in the performance of the AEV burners placed in the SGT−800.

The SGT−800 is a single shaft gas turbine with 30 burners of AEV type and generates approximately 40 MW.

2.1 Purpose

With the chemical reaction software Chemkin 4.0 as a tool the ignition temperature, adiabatic flame temperature, NO_X emissions and laminar flame speed were studied for natural gas with different composition. To simulate the conditions in the AEV burner different types of reactor models were used.

A definition of the problem was made by assuming that the reaction course could be described using one single reactor, not combining different models. Furthermore the turbulent flame speed was not studied.

3 General combustion equations

The reaction of one mole of fuel, F, with a moles of oxidizer, Ox, forming b moles of combustion products, Pr, is expressed by the global reaction mechanism

$$F + aOx \rightarrow bPr. \tag{1}$$

From experimental measurements the rate at which the fuel is combusted, i.e. rate of reaction for the fuel, can be expressed as eq.(2).

$$\frac{d\left[X_F\right]}{dt} = -k_G(T)\left[X_F\right]^n\left[X_{Ox}\right]^m \tag{2}$$

X_F is the molar concentration of the fuel, X_{Ox} the molar concentration of the oxidizer and k_G the global rate coefficient. The exponent n and m relates to the reaction order and are together with the global rate coefficient retrieved from curve fitting experimental data.

The global reaction mechanism, eq.(1), simplifies the reaction course and does not display the reactions where the many intermediate species are formed. In reality for eq.(1) to be true all the a molecules of the oxidizer should collide at the same time with the fuel molecule and form b product molecules. This is unrealistic and the reaction should instead be described by several reactions, so called elementary reactions, including the intermediate species resulting in a so called reaction mechanism. One example is the global reaction for formation of water.

$$2\,\mathrm{H_2} + \mathrm{O_2} \longrightarrow 2\,\mathrm{H_2O}$$

In this reaction the following reactions with intermediate species are also important

$$\begin{aligned}
\mathrm{H_2} + \mathrm{O_2} &\longrightarrow \mathrm{HO_2} + \mathrm{H} \\
\mathrm{H} + \mathrm{O_2} &\longrightarrow \mathrm{OH} + \mathrm{O} \\
\mathrm{OH} + \mathrm{H_2} &\longrightarrow \mathrm{H_2O} + \mathrm{H} \\
\mathrm{H} + \mathrm{O_2} + \mathrm{M} &\longrightarrow \mathrm{HO_2} + \mathrm{M}
\end{aligned}$$

among others.

H, O, OH and $\mathrm{HO_2}$ are reactive molecules with unpaired electrons, so called radicals.

The reaction when two molecules collide and react into two different molecules, a bimolecular reaction, is expressed as:

$$A + B \underset{k_r}{\overset{k_f}{\rightleftharpoons}} C + D \tag{3}$$

Where k_f and k_r are the forward and reverse rate coefficients.

The reaction rate of species A is proportional to the concentrations of the two reacting species as

$$\frac{d\,[A]}{dt} = -k_f\,[A]\,[B] + k_r\,[C]\,[D] \tag{4}$$

The rate constants, k_f and k_r, in eq.(4) are described numerically by Arrhenius in the Arrhenius temperature dependence equation, eq.(5). The Arrhenius temperature dependence equation gives the relation between the rate constant and the temperature, T.

$$k_{fi} = A_i T_{\beta_i} e^{(\frac{-E_i}{R_c T})} \tag{5}$$

where A_i is the frequency or pre-exponential factor which can be interpreted as the fraction of reacting molecules to the total number of colliding molecules with sufficient kinetic energy to cause a reaction. β_i the temperature exponent, E_i the activation energy, the energy required for reaction to occur as a result of the collision, R_c the universal gas constant with units consistent with the activation energy and i is the different reactions. Here eq.(5) is solved for k_f but the equation for k_r is the same with different A_i, β_i and E_i.

When $\frac{d[A]}{dt} = 0$, i.e. steady state, the relation between the forward and reverse rate constants is given by an equilibrium constant, K_{ci}, shown in eq.(6).

$$k_{ri} = \frac{k_{fi}}{K_{ci}} \tag{6}$$

The subscript c indicates that the definition is based on concentrations.

In many cases a third body, which consumes, or contributes with kinetic energy, is required for the reaction to proceed. This is often the case in dissociation or recombination reactions for example

$$\mathrm{H} + \mathrm{O_2} + \mathrm{M} \longrightarrow \mathrm{HO_2} + \mathrm{M}$$

The species production rate, $\dot{\omega_k}$, is defined in eq.(7).

$$\dot{\omega_k} = \sum_{i=1}^{I} \nu_{ki} q_i \tag{7}$$

where ν_{ki} is the stoichiometric coefficient and the difference of ν'_{ki} and ν''_{ki}, $\nu_{ki} = \nu''_{ki} - \nu'_{ki}$

The rate-of-progress variable, q_i included in equation 7, is expressed in eq.(8)

$$q_i = (\sum_{k=1}^{K}(a_{ki})\,[X_k])(k_{fi}\prod_{k=1}^{K}[X_k]^{\nu'_{ki}} - k_{ri}\prod_{k=1}^{K}[X_k]^{\nu''_{ki}}) \tag{8}$$

X_k is the molar concentration of kth species, ν'_{ki} is the coefficient for reactant and ν''_{ki} is the stoichometric coefficient for the product species including the forward and backward rate coefficients. Subscripts i and k refers to the ith reaction and kth species.

The difference influence from third body reactions are accounted for by the factor including a_{ki}. If all the species contributes equally as third bodies a_{ki} is equal to one and the factor is the total concentration of the mixture which also equals one.

These are some of the basic kinetic equations used as base in the following equations for the chemical reactors [1].

4 Reactor models

4.1 PSR - Perfectly Stirred Reactor in theory

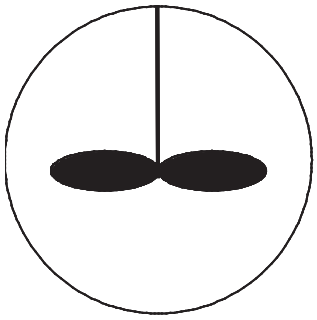

Figure 1: A theoretical perfectly stirred reactor.

The perfectly stirred reactor is an ideal chemical reactor in which perfect mixing is achieved inside the control volume. This means that the composition within the reactor is everywhere the same [**1**].The gas from the inlet is instantly mixed with the existing reactor content and the composition in the outlet will be the same as in the reactor, so called back mixing [**2**]. The mixture in a perfectly stirred reactor is blended with the combustion products and heated so quickly that in passing through the chamber with a sampling probe it is difficult to locate any regions with composition or temperature different than in other regions. Due to intense recirculation in the chamber, no defined directions of the flow can be distinguished either [**3**].

4.2 Basic equations in the PSR model

In addition to fast mixing, the modeling of homogenous reactors requires several assumptions. The mass transport into and within the reactor is assumed to be infinitely fast and the flow through the reactor must be characterized by a nominal residence time. For open systems the pressure is specified so that the conservation equations determine the volume outflow. The assumptions made in this study are only one reactor, i.e. no recirculation, no surface reactions and only one inlet into the system.

The continuity equation, eq.(9), expresses the change in mass over the volume V

$$\frac{d}{dt}\int_V \rho(\overrightarrow{x},t) = -\int_\Gamma \rho v_n \hat{n} dA \tag{9}$$

The condition "no surface reactions" mentioned earlier results in a constant volume. The mass balance equation is then reduced to eq.(10). The equation states that the time-rate change of the mass in the reactor is equal to the difference between the mass flow in and the mass flow out.

$$V\frac{d\rho}{dt} = \dot{m}^* - \dot{m} \tag{10}$$

where ρ is the density, V is the reactor volume and $\dot{m}$ the mass flow. The superscript * indicates the inlet and no superscript indicates the outlet. Since the density is constant the inlet mass flow equals the outlet mass flow, i.e. stationary flow.

The species conservation equation reduces to eq.(11) when applying the assumptions mentioned above. The equation describes the change in composition within the gas.

$$\rho_k V\frac{dY_k}{dt} = \dot{m}(Y_k^* - Y_k) + \dot{\omega}_k V W_k \tag{11}$$

Where Y_k is the mass fraction, $\dot{\omega}$ is the molar rate production by gas-phase chemical reaction per unit volume and W_k the molecular weight. The subscript k indicates the k th species.

Eq.(12) defines the residence time τ under the conditions mentioned earlier.

$$\tau = \frac{\rho V}{\dot{m}} \tag{12}$$

The energy balance is determined by considering a control volume that includes the reactor and all walls and materials therein. This results in the gas energy equation, eq.(13).

$$\frac{dU_{sys}}{dt} = \dot{m}\Big(\sum_{k=1}^{K_g}(Y_k^* h_k^*) - \sum_{k=1}^{K_g}(Y_k h_k)\Big) - Q_{source} - Q_{loss} \tag{13}$$

Where U_{sys} is the total inner energy, h_k the specific enthalpy, Q_{source} the reaction energy, energy from reactions taking place inside the reactor, and Q_{loss} is the net heat flux directed from the reactor. Since the reactor studied here is adiabatic the term Q_{loss} is set to zero **[5].**

4.3 Well Stirred Reactor - Perfectly Stirred Reactor in reality

In reality no reactor, despite extremely intensive mixing, is perfectly stirred and the attempt to resemble such a reactor is therefore often called a well stirred reactor **[3].**

One reactor used as a PSR in experiments is the Longwell-reactor. The Longwell-reactor, shown in figure 2, is a reactor where the mixing rate is much faster than the reaction rate. The spherical chamber is lined with an insulating fire brick to minimize heat losses. Premixed fuel and air enter at sonic velocity through jets aimed at the center and hot combustion products leave through pores in the brick **[6]**.

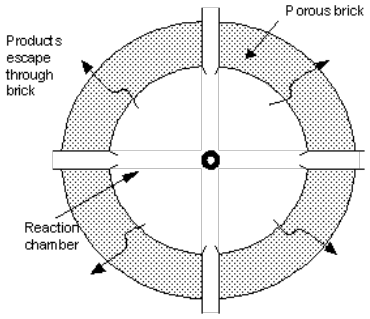

Figure 2: The Longwell reactor.

4.4 PFR - Plug Flow Reactor

The second type of reactor used in reactor engineering is the plug flow reactor , PFR, see figure 3.

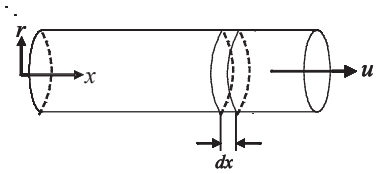

Figure 3: PFR.

The plug flow reactor is essentially a perfectly stirred reactor without any back mixing [**4**]. In the plug flow reactor the complete mixing is assumed in the radial direction and no back mixing is presumed in the flow direction, this means that the composition at a certain distance from the inlet is the same independent of the radial distance to the wall, no back mixing occurs. As a result, the profiles of velocity, temperature and composition are flat in every cross sectional normal to the flow, and the composition changes only along the flow, according to chemical kinetics and turbulence [**3**].

For the plug flow reactor the following assumptions are made:

- Steady-state, steady flow
- No mixing in the axial direction. This implies that molecular and/or mass diffusion is negligible in the flow direction.
- Uniform properties in the direction perpendicular to the flow, i.e. one dimensional flow. This means that at any cross-section, a single velocity, temperature or composition completely characterizes the flow.
- Ideal frictionless flow. The assumption allows the use of the simple Euler equation to relate pressure and velocity
- Ideal-gas behavior. eq.(14), the ideal gas law can be used. [**1**]

$$p\frac{1}{\rho} = \sum_i n_i RT \tag{14}$$

Where n_i is the number of molecules of the species i and R the gas constant.

The equations governing the behavior of a plug flow reactor are simplified versions of the general relations for conservation of mass, energy and momentum. They can be derived by writing balances over a differential slice in the flow direction with the conditions that there are no variations in the transverse direction and that the axial diffusion of any quantity is negligible relative to the corresponding convective term. Additionally an assumption of no surface reactions is made.

With the assumptions above the mass balance is expressed as in eq.(15). The equation states that the mass flow rate is not changed inside the reactor. Since A is allowed to change with x the properties need to be constant for every x for the flow to still be one dimensional.

$$\rho u\frac{dA}{dx} + uA\frac{\rho}{dx} + \rho A\frac{u}{dx} = 0 \tag{15}$$

With the assumptions made above, and the assumption that with no surface reactions occur the area is constant, the gas species conservation equation is expressed as in eq.(16). The equation describes the change in the composition of the gas and is correspondingly to the PFR as eq.(11) is for the PSR.

$$\rho uA\frac{dY_k}{dx} = W_k\dot{\omega}_k A \tag{16}$$

Eq.(17), the energy equation, states that the total energy of the flowing gas changes due to the heat flux Q_e from the surroundings to the outer tube wall and also due to accumulation of enthalpy in the bulk solid.

$$\rho uA\Big(\sum_{k=1}^{K_g} h_k\frac{dY_k}{dx} + \overline{c}_p\frac{T}{dx} + u\frac{du}{dx}\Big) = a_e Q_e. \tag{17}$$

$\overline{c}_p$ is the mean heat capacity per mass and $a_e$is the surface area per unit length of the outer tube wall.

The momentum equation, eq.(18), expresses the relation between the pressure forces, inertia and the viscous drag.

$$A\frac{dp}{dx} + \rho uA\frac{du}{dx} + \frac{dF}{dx} = 0 \tag{18}$$

p is the absolute pressure and F is the friction force exerted on the gas by the tube wall. [**1**]

4.5 Premixed Laminar Flame-Speed

The third model used in this study is the premixed laminar flame-speed model.

The definition of a deflagration flame according to reference [**1**] is a self-sustaining propagation of a localized combustion zone at subsonic velocities. This means that the flame needs to be localized, i.e. the flame occupies only a small portion of the combustible mixture at any one time. The flame also needs to be subsonic.

In figure 4(a) a long pipe with constant cross section has in one end a propagating flame and a premixed gas flowing towards the combustion zone. The laminar flame speed, S_L, is equal to the velocity of the gas mixture far upstream, beyond all influence of the flame zone, where ρ_∞, T_∞ and $u_\infty = S_L$ exists.

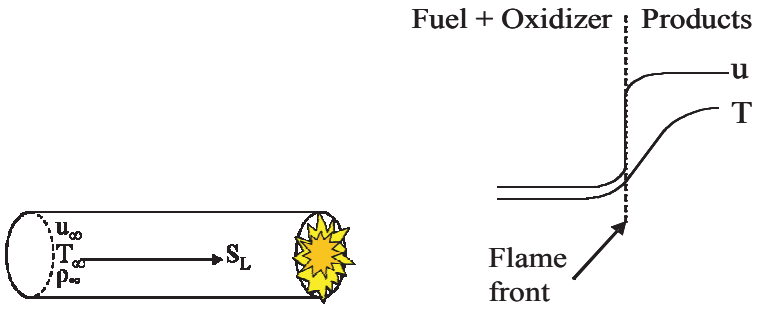

(a) (b)

Figure 4: a) Laminar flame speed model. b) Propagation of a laminar flame.

Figure 4(b) shows the temperature and velocity in the flame and flame front, on the left hand side the fuel is uncombusted and the velocity $u = S_L$, the fuel and oxidizer then enters the flame front and is combusted. On the right hand side the velocity has increased due to the increase in density when the fuel is combusted. The velocity u no longer equals the laminar flame speed. When the premixed gas is flowing at the laminar flame speed, S_L, the flame is stable. A stable flame is not moving upstreams, i.e. flashback, or pushed out, i.e. blow off.

The assumptions made for this theoretical laminar flame are

- One-dimensional, constant area, steady flow
- Kinetic and potential energies, viscous shear work and thermal radiation are all neglected.
- Constant pressure, the pressure difference across the flame is neglected
- Binary diffusion is assumed.
- The Lewis number, Le, expressing the ratio between thermal and mass diffusivity, eqn 19, is equal to one.

$$Le \equiv \frac{\alpha}{D} = \frac{k}{\rho c_p D} \tag{19}$$

where D is the mass diffusivity.

- The oxidizer is present in Φ=1 or below proportions, the fuel is completely consumed at the flame front.

According to reference **[1]** the governing conservation equations for mass, species and energy are then expressed as:

The mass conservation equation

$$\dot{m} = \rho u A \tag{20}$$

The species conservation equation

$$\frac{d}{dx}\Big(\dot{m}Y_k - A\rho D\frac{dY_k}{dx}\Big) = \dot{\omega}_k W_k A \tag{21}$$

Energy conservation equation

$$\dot{m}c_p\frac{dT}{dx} - \frac{d}{dx}\Big((A\rho c_p D)\frac{dT}{dx}\Big) = -A\sum_{k=1}^{K}\dot{\omega}_k h_k W_k \tag{22}$$

5 The Advanced Environmental Vortex burner

Figure 5 shows the SGT−800 with its 30 burners of Advanced Environmental Vortex, AEV, type. The SGT−800 is a single shaft gas turbine, where the air enters from the left in figure 5, passes through the compressor and entering the burners where the fuel is added, explained more thorough later in the chapter. The hot gas leaving the combustion chamber then forces the turbine to rotate by expanding. The gas then leaves through the outlet diffuser.

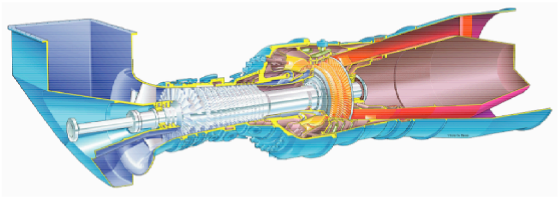

Figure 5: SGT-800

The gaseous fuel enters the burner through the main gas pipes which are placed on a swirl cone, as seen in figure 6. The mixing of the gas and air is initiated in the slots in the cone which is called a swirl generator. The gas is injected through holes in the main gas pipes. The mixing then continues in the mixing tube where the fuel and air are mixed to a homogeneous mixture.

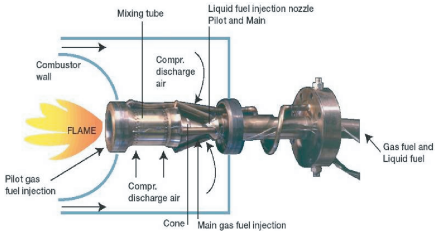

Figure 6: The AEV burner

Figure 7 shows the distribution of the air in the AEV burner. As seen 85 % enters through the cone slots of the burner and 10% enters the mixing tube through four rows of small holes, called film holes, in the mixing tube. 3% of the remaining airflow enters in the center of the burner and the remaining 2% participates in the combustion in the pilot flame.

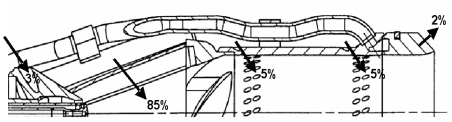

Figure 7: Distribution of air in the AEV burner.

5.1 Velocities in the AEV burner

The back of the AEV burner is placed between the outer and inner central casing while the front is placed in the combustion chamber. When the air enters the space between the inner- and outer central casing the velocity is tangential and therefore easily enters the cone slots on the burner. The slots generate a swirl with a tangential velocity approximately twice the axial velocity which mixes the air with fuel from the main gas pipes. The pressurized fuel is transported in separate pipes for main- and pilot gas.

In the mixing tube the highest velocity will be at the center, see figure 8 , the high velocity will prevent the gas-air mixture to pre-ignite. The air from the film holes in the mixing tube keeps the gas from the walls. This prevents the gas from igniting in the mixing tube causing a so called flashback.

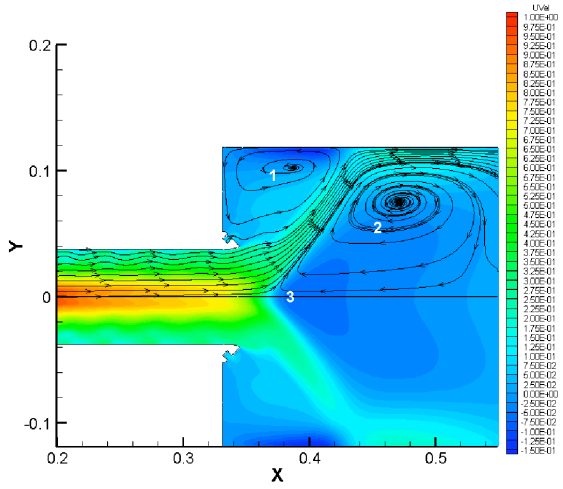

Figure 8: Normalized axial velocities in the mixing tube and combustion chamber. Recirculation zone 1 is marked 1 and recirculation zone 2 marked 2

When the fuel- air mix enters the combustion chamber an expansion occur, forming two recirculation zones, marked 1 (outer) and 2 (inner) in figure 8 . Recirculation zone 2 is actually caused by the vortex breakdown which is a result of the expansion of the swirling flow. In the point where the recirculated flue gases meet the uncombusted premixed gas a stagnation point forms, marked 3 in figure 8 . The forces caused by the swirl contribute to recirculation zone 2. The ratio between the axial and tangential velocities in the swirl is called the swirl number.

Recirculation zone 2 is the main contributor to the flame stabilization by the vortex bubble created by the hot recirculated combustion gases helping the gas to ignite. Stabilization of the flame is also contributed by recirculation zone 1. The flame is placed between recirculation zone 1 and 2. The swirl number is very important for the flame. If the axial velocity in the swirl is to small the stagnation point, and thus the flame, is drawn backwards into the mixing tube causing flashback. If the axial velocity is too high the flame will be pushed out into the combustion chamber, burn off, and is thereby not stable. The pilot

flame is supposed to support the main flame and thus it is desired that the pilot flame enters between recirculation zone 1 and the main flame.

5.2 Temperatures in the AEV burner

Figure 9 shows the temperatures in the AEV burner. The figure is taken from a simulation in Fluent with pure methane as fuel. The figure will change with different fuels and load but gives an idea of the temperatures in the burner and combustion chamber. The highest temperature, about 2000 K, is found near the flame. In the mixing tube the temperature is 650 K explained by the temperature of the air from the compressor. The exhaust gas leaving the combustion chamber has a temperature of about 1800 K.

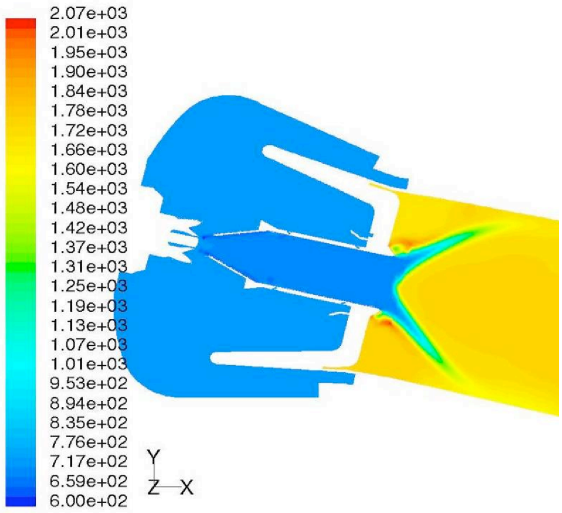

Figure 9: Temperatures [K] in the AEV burner and combustion chamber

6 Chemkin

6.1 PSR model in Chemkin

In Chemkin the PSR consists of a chamber, which may or may not allow heat loss, with inlet and outlet ducts. The assumptions made for the reactors used in Chemkin are: only one reactor in the system, no surface reactions and only one inlet. Since there is only one reactor no recirculation can occur.

In Chemkin the user can either specify the gas temperature or request the temperature as a solution of the energy equation in the reactor.

6.2 PFR model in Chemkin

The tube flow configuration is a natural choice for processes that are carried out in a continuous fashion. For this reason, such reactors are usually operated at steady state. Since the general equations for chemically reacting flow involve transport phenomena in addition to kinetics and thermodynamics, rigorous reactor models are by necessity multidimensional. However, there are often practical and mathematical reasons for considering idealized dimension reduced models. This idealization results in a plug flow reactor described earlier. The equations used by Chemkin in the PFR are described in a previous chapter.

6.3 Premixed Laminar Flame-Speed model in Chemkin

The premixed laminar flame-speed model is unlike the PSR and PFR models not a reactor model but a calculation model for the premixed laminar flame speed.

The model solves the set of governing differential equations that describes the flame dynamics using implicit finite difference methods as well as a combination of time dependent and steady state methods.

The premixed laminar flame speed calculation model involves a freely propagating flame. The pressure and inlet temperature are specified and there are no heat losses. The temperature can is solved by the energy equation. The calculation time can be reduced if an estimation of the temperature is made. The flame speed is then calculated.

6.4 Numerical solver in Chemkin

The numerical solver in Chemkin allows the user to choose the tolerances. Depending on what system that is to be studied, the time constants of the system and what reactions are to be studied the numerical tolerances need to be adjusted.

The reactions used in the system are relatively fast. This means that the time for the temperature of the fuel-air mixture in the system to change from inlet temperature to the temperature of a burning flame is small. The fraction of radicals (short lived, reactive, intermediate species) is therefore influential even at concentrations as low as 1 ppm.

The default tolerances are in most cases adequate but when looking at species with mol fractions as small as 1E-9 the tolerances need to be adjusted. The adjusted tolerances are shown in table 1. The tolerances were determined by

decreasing in steps by the factor 1E-1 until no difference in the solution could be observed.

The "relative tolerance" indicates how many significant digits the converged solution contains. The "absolute tolerance" is set as the smallest number a solution component can have without being excluded from the relative convergence criteria. "Relative tolerance for pseudo time stepping" is the relative tolerance for convergence when pseudo time stepping, change in the time stepping for easier convergence, is used. The "minimum bound on species fraction" is set to a small negative number to give the solver a larger interval to search for a solution. "Positive value to reset" is the value to be set when the species concentration becomes negative, i.e. unphysical, during the iteration.

	Default	Corrected
Absolute tolerance	1E-9	1E-14
Relative tolerance	1E-4	1E-10
Relative tolerance for pseudo timestepping	1E-4	1E-6
Minimum bounds on species fraction	-1E-4	-1E-6
Positive value to reset	-1	1E-20

Table 1: The adjusted tolerances and the original values in the numerical solver in Chemkin.

7 Chemical reaction mechanism study

Four chemical reaction mechanisms were evaluated with Chemkin to be used for ignition prediction in the AEV burner. A summary of the mechanisms can be seen in table 2. For a complete list of all the species represented in each mechanism see appendix A.

Mechanism	I	II	III	IV
Number of species	73	53	151	546
Number of reactions	520	325	939	2446
Hydrocarbons represented	CH_4 - C_2H_6	CH_4 - C_3H_8	CH_4 - C_4H_{10}	CH_4 - C_7H_{16}
Reference	[8]	[9]	[10]	[11]

Table 2: Number of species, reactions and hydrocarbons represented in the different mechanisms. For a more thorough description of the species represented see appendix A

To evaluate the mechanisms stoichiometric combustion of either pure methane or pure ethane in a PSR with fixed gas temperature were simulated. As oxidizer air was used. These fuels were chosen since mechanism I only includes hydrocarbon species up to ethane.

For each residence time several simulations were made at the pressures 1 and 20 bar to determine the accuracy of the mechanisms in atmospheric as well as pressurized systems.

It would have been preferable to use experimental data as guidance when choosing the mechanisms. Unfortunately no data consistent with the case of our interest was found. Instead we assume that the most extensive mechanism (including the largest number of species and reactions) also has the best capability to simulate our case of natural gas combustion. This mechanism, mechanism IV, has according to litterature, been tested successfully up to 40 bar [**11**].

The aim with the mechanism study was to find an alternative, faster, mechanism to mechanism IV. Since higher number of species and reactions in the mechanism need more computational time during the simulations only mechanisms with less reactions and species than mechanism IV where chosen for the study. The relation between number of reactions and computational time was though not true in all cases. Table 2 shows that mechanism IV has almost three times as many reactions as mechanism III, however despite fewer reactions the simulation with mechanism III takes longer time due to convergence difficulties.

7.1 Methane as fuel

Figure 10(a) and figure 10(b) show concentration, or mol fraction, in volume percent CH_4 as a function of temperature with the residence time, τ, 1 ms and the fuel to air ratio, Φ=1 at 1 and 20 bar respectively.

The simulations with methane as fuel show that mechanism I needs the highest temperature to start reacting. The "smooth curve" in the beginning

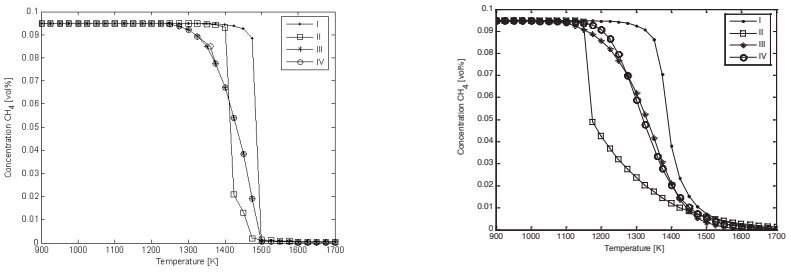

(a) (b)

Figure 10: Combustion of methane with τ=1ms, Φ=1 and a) p=1 bar and b) p=20 bar.The figure shows the change in concentration of methane with different mechanisms. The different mechanisms are marked with different dots.

resembles the curve from the simulations with mechanisms III and IV until about 10% of the initial methane has reacted. Then a steep slope follows as the temperature rises 20 degrees more, to 1500 K and all methane is burnt.

Mechanism II is the mechanism that differs most from the others. Figure 10(a) and figure 10(b) show that mechanism II is more sensitive to pressure, the methane combusts very rapidly and that the conversion rate of methane doesn't resemble the other mechanisms. The fast combustion in the beginning resembles an explosion which doesn't occur for any of the other mechanisms.

Mechanisms III and IV have only one data point that differ at the pressure 1 bar. At 20 bar, figure 10(b), the difference increases but the mechanisms still have a strong resemblance.

7.2 Ethane as fuel

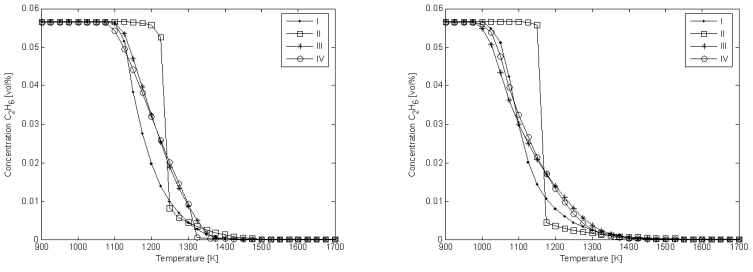

(a) (b)

Figure 11: Combustion of ethane at τ=1 ms, Φ=1 at a) p=1 bar and b) p=20 bar. Concentration of ethane as a function of temperature. The different dots show the different mechanisms.

Figure 11(a) and figure 11(b) show the concentration of ethane as a function of temperature. As seen in the figures mechanism II is again the mechanism that differs most from the other mechanisms. The temperature necessary for

the reaction to start with mechanism II is higher than for the other mechanisms and the combustion, when started, is very fast.

For ethane combustion mechanisms I, III and IV show similar behavior. The three mechanisms have almost the same ignition temperature and combustion rate (inclination of the curve). As shown in both figure 11(a) and figure 11(b) mechanism I needs a significantly higher temperature than the other mechanisms to react when pure methane combustion is considered but when combusting ethane the temperature is almost the same for mechanisms I, III and IV.

Figure 12(a) and figure 12(b) show the mol fraction of methane as a function of temperature. Figure 12(b) show that at 20 bar and the residence time 1 ms the production of methane, due to combustion of ethane, increases at the same temperature for mechanisms III and IV and at a slightly higher temperature for mechanism I. Mechanism II however needs an additional 150 K to the temperature required with mechanism III and IV to start increasing the fraction of methane. The fraction methane produced is almost the same for mechanisms II, III and IV. The higher fraction produced by mechanism I could be due to that mechanism I only produces methane during the combustion while the other mechanism can produce higher hydrocarbons.

The influence of pressure is seen by comparing figure 12(a) and figure 12(b). At 20 bar the concentration of methane decreases for mechanisms I and II while the fraction increases for mechanisms III and IV. Mechanism II seems to be the one differing most when pressurized. The fraction of methane at 20 bar is reduced to almost one tenth of its value at 1 bar. When increasing the residence time to 10 ms the methane concentration at 1 bar, shown in figure 13(b), is almost the same for mechanisms I, III and IV. Mechanism II however still differs both in the size of maximal mol fraction of methane and the temperature for which the concentration of methane peaks.

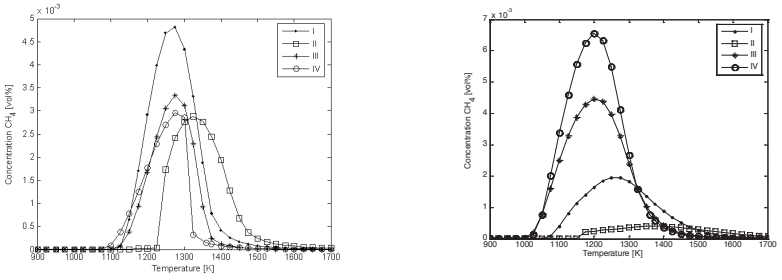

(a) (b)

Figure 12: Production of methane when combusting ethane at τ=1 ms, Φ=1 at a) p=1 bar and b) p=20 bar.

Figure 13(a) and figure 13(b) show the methane concentration at 1 bar and 20 bar respectively with the residence time 10 ms. At this longer residence time the resemblance for mechanisms I, III and IV increases for 1 bar while when pressurized to 20 bar the resemblance decreases when comparing figure 12(b) and figure 13(b).

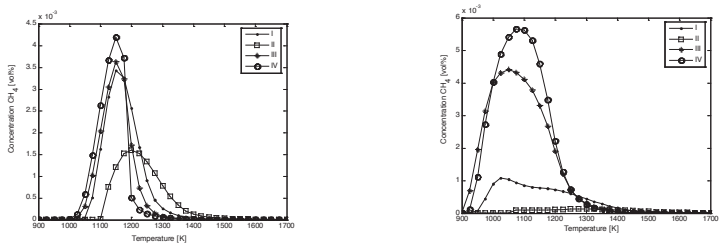

(a) (b)

Figure 13: Production of methane when combusting ethane at τ=10 ms, Φ=1 at a) p=1 bar and b) p=20 bar.

7.3 Conclusion

When comparing the simulations with different pressures mechanism II is the most deviating when increasing the pressure.

Another observation made when combusting pure methane is that mechanism I needs a significantly higher temperature than the other mechanisms to react, but when combusting ethane the temperature is almost the same for mechanisms I, III and IV. The conclusion is therefore that results using mechanism I should be treated carefully with fuels that consist only of methane and no larger hydrocarbons.

Adding the results from simulations with both fuels the conclusion is made that mechanism II is the mechanism that differs most from the other. Mechanisms III and IV are the most similar ones. The purpose of the study was to find a faster alternative to mechanism IV. Since mechanism III had convergence problems the most appropriate mechanisms to continue the simulations with are mechanisms I and IV.

8 Gases used in the simulations

The simulations where made with natural gas of three different compositions. Table 3 shows the compositions of the gases used in the simulation. The compositions are taken from gas analyses done by AGA [**7**].

Gas	A	B	C
He	0.0396	0.0035	0.0132
N_2	10.12	0.328	0.871
CO_2	1.506	1.158	0.094
CH_4	82.84	88.38	97.76
C_2H_6	4.098	6.291	0.8615
C_3H_8	0.9615	2.631	0.2821
$n-C_4H_{10}$	0.17	0.575	0.0481
$i-C_4H_{10}$	0.136	0.399	0.465
$n-C_5H_{12}$	0.0396	0.077	0.0084
$i-C_5H_{12}$	0.0329	0.107	0.0094
C_6H_{14}	0.0177	0.0251	0.0049
C_6H_{12}	0.0209	0.0091	0.0007
C_7H_{16}	0.0076	0.0055	0.0006
C_7H_{14}	0.0043	0.0031	0.0007
C_8H_{18}	0.0029	0.0004	–
Density [kg/m^3]	0.7345	0.8330	0.8383
Calorific value superior [MJ/m^3]	39.98	43.96	37.44

Table 3: Composition of the different gases used in the simulations.

When comparing the gas compositions the most obvious differences are the high nitrogen fraction in gas A and the high fraction of methane in gas C. The fraction of methane in gas A is lower than both gas B and C. The density also differs between the gases. Gas B and C have almost the same density while gas A has a density that is approximately 10 percent higher than gas B and C.

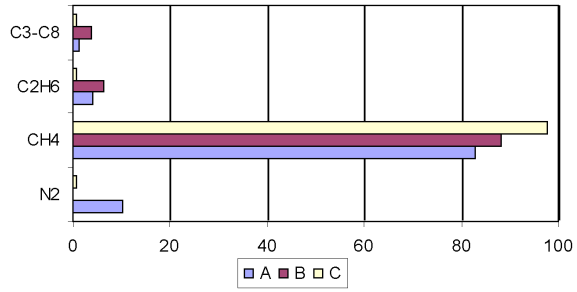

Figure 14: Composition of gas A, B and C. The hydrocarbons with three carbon atoms or more are amalgamated into one bar.

Figure 14 shows that gas B has the highest fraction of both ethane and

hydrocarbons with three carbon atoms and more.

Since the highest hydrocarbon represented in mechanism I is ethane the gases were recalculated when using this mechanism. The hydrocarbons higher than ethane were transformed into ethane by calculating the number of carbon atoms in the higher hydrocarbons and replacing them with the equivalent amount of ethane. For instance C_4H_{10} is converted to two C_2H_6 molecules. The increased number of hydrogen molecules from 10 to 12, results in an error in the simulations that is not a result of the code in the mechanism.

9 Fixed gas temperature

9.1 Definition of ignition and burnout temperature

The simulations to define ignition and burnout temperature were made both with a PSR and a PFR. Since simulations with both reactors gave the same results only the simulations with the PSR are shown here.

One of the first radicals to be produced when combustion initiates is the HO_2 radical. To define an ignition temperature a comparison between the concentration of methane and HO_2 is made.

The lower figure in figure 15 shows the mol fraction of HO_2 as a function of temperature and the upper one of the figures shows the concentration CH_4 as a function of temperature. When comparing both the figures it is observed that the sudden increase in concentration HO_2 occurs at the same temperature as the mol fraction of CH_4 begins to decrease. It is concluded that the ratio between the concentration and inlet concentration of methane is a way to determine the ignition temperature.

The ignition temperature is set where the concentration ratio of methane is below 95% which is shown in figure 15. The burn out temperature is defined in the same way for concentration ratio of methane below 5%, also shown in figure 15.

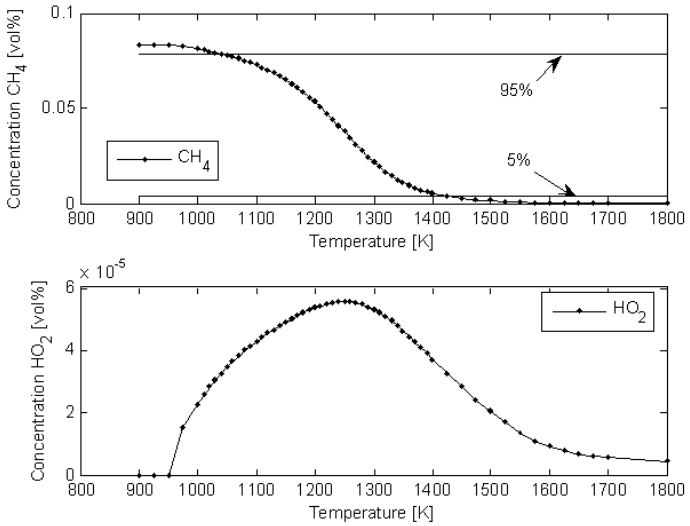

Figure 15: Definition of the ignition and burnout temperatures (above). Production of the HO2 radical (below).

9.2 Simulations in a PSR

When simulating the PSR with a fixed gas temperature the energy equation is not used. The gas enters the reactor with a temperature, which remains constant throughout the reaction, the reaction then proceeds until the residence time has elapsed and the state is then frozen. This gives a picture of how the required temperature for a reaction varies with the residence time.

Residence time	1, 3, 10, 20, 30 ms
Volume	0.00033 m^3
Temperature	800 − 2200 K
Pressure	20 bar
Φ	0.5, 1

Table 4: Conditions set in the PSR for the different simulations.

The settings used for simulations with a fixed gas temperature are shown in table 4. The conditions set for the simulations fit the conditions in the AEV burner. The two shortest residence times were chosen to fit the residence times in the AEV burner while the other three are relevant since some reactions need long residence times to occur. Since the reactor is isothermal and perfectly stirred the volume has no influence on the simulations. In total 960 simulations were made.

Figure 16 shows the influence of residence time, τ, and fuel/air ratio, Φ, on the temperature where the reaction initiates. For both the mechanisms the temperature for initiated reaction decreases with increasing τ and decreasing Φ as can be seen in figure 16. The concentration of methane decreases with decreasing Φ since the amount of air in the mixture increases.

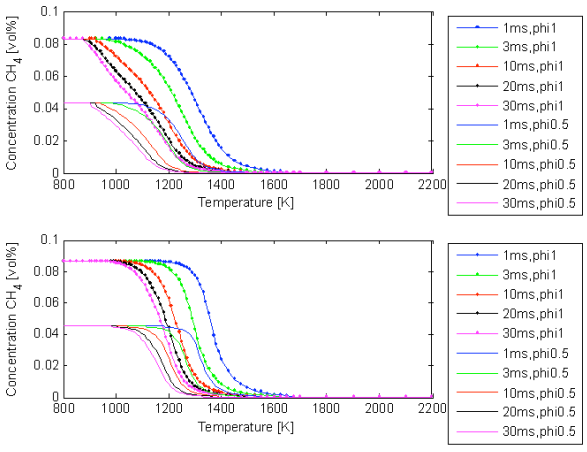

Figure 16: Combustion of gas A with mechanism IV (above) and mechanism I (below). The lines with dots represent Φ=1 and the lines without dots Φ=0.5.

9.2.1 Comparison of gas A, B and C

Simulations were made for all tree gases with the parameters shown in table 4 and with both mechanism I and IV.

Mechanism IV As seen in figure 17 gas C needs a slightly higher temperature to react, followed by A and B.

Figure 18 the ignition and burnout temperatures as functions of the residence time are shown. The distance between the curve for the ignition and the burnout temperature shows the rate of which the gases react, this represents the slope of the curve in figure 17.

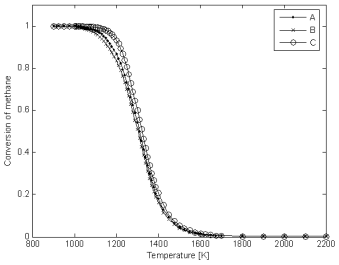

Figure 17: Combustion of gas A, B and C (represented with different dots) with p=20 bar, Φ=1 and τ=1 ms.

Figure 18 shows that the largest difference, between all three gases, is at the residence time 1 ms with Φ=1 and as the residence time increases the difference between the gases decrease. Comparing the two figures in figure 18 one can see that the difference between gas A and B decrease with lower Φ.

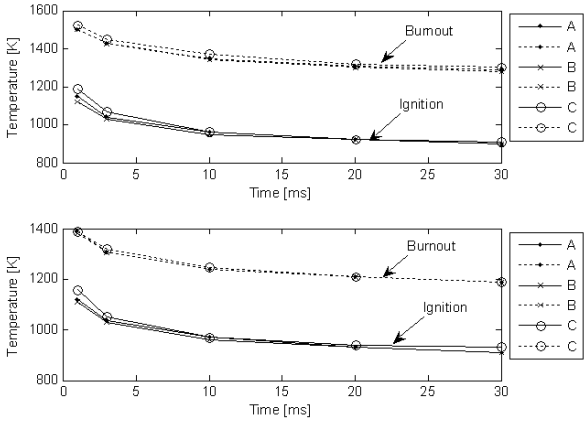

Figure 18: Combustion of gas A, B and C at Φ=1 (above) and Φ=0.5 (below). The ignition, lines, and burnout, dotted lines, temperatures are shown as a function of residence time.

The gas that differ the most is gas C. At the residence time 1 ms and Φ=1 the gas needs a temperature that is 50 degrees higher than for gas A and 80 degrees higher than for gas B to ignite. Also the difference between ignition and burnout is smaller which indicates a faster combustion than in gas A and B.

For Φ=0.5 the difference in ignition temperature between gases A and B is negligible. The ignition temperature as well as the burnout temperature decreases which results in an unchanged reaction rate. The higher temperature needed for gas C to ignite however still remains.

With decreasing Φ the ignition and burnout temperatures decreases for all the gases. The reason is that with Φ=1 the methane fraction in the mixture is higher than with Φ=0.5. A high methane fraction consumes the radicals and thereby slows down the combustion which results in higher ignition temperatures. This is also explained by the exponent m in eq.(2) , which for methane is negative and then results in a decreased reaction rate for increased fraction of methane.

Mechanism I Figure 19 shows the results from the simulation under the conditions 1ms and Φ=1 with mechanism I. Here gas A and C seems to ignite at the same temperature while gas B ignites at a lower temperature. Comparing figure 18 and figure 19 it is seen that all gases have a higher ignition temperature with mechanism I.

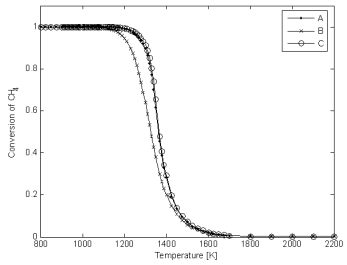

Figure 19: Combustion of gas A, B and C for Φ=1 and τ=1ms.

A comparison of figure 18 and figure 20 include all the residence times.

Comparing the mechanisms at all residence times (figure 18 and figure 20) one can observe that the ignition temperature of gas A with Φ=1 differs 120 degrees between the mechanisms while gas B and C only differs 75 degrees. The burnout temperatures does not change as much, for Φ=1 the burnout temperature is only 10 degrees higher for mechanism I. The combustion rate is then higher for mechanism I than for mechanism IV.

The mechanism change with the recalculation of the hydrocarbons changes the composition of gas B the most. Despite this it is the ignition temperature for gas A that changes the most. The ignition temperature for gas A at Φ=1 with mechanism I is 120 degrees higher than with mechanism IV while gas B and C only change 75 degrees. The change in ratio between ethane and methane due to recalculation of the gas is the biggest for gas A and this could be one reason for the big change in ignition temperature.

With Φ=0.5 the ignition temperature increases with 150 degrees for gas A with mechanism I instead of mechanism IV. The ignition temperature for gas B increases 80 degrees and for gas C the increase is 85 degrees. With mechanism I the burnout temperature increases 50 degrees which also increases the combustion rate for the mechanism.

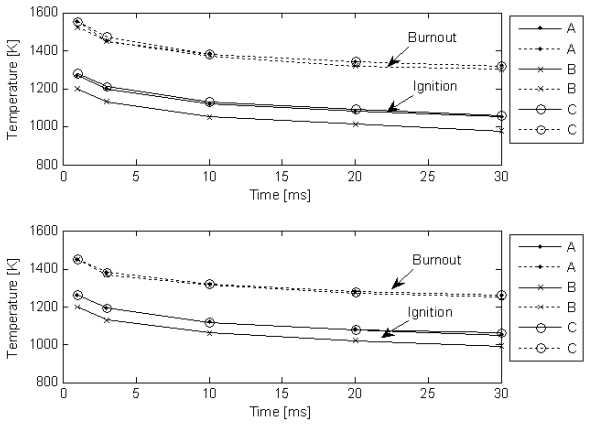

Figure 20: Combustion of gas A, B and C at Φ=1 (above) and Φ=0.5 (below). The ignition, lines, and burnout, dotted lines, temperatures are shown as a function of residence time.

9.3 Simulations in a PFR

Length	0.6 m
Residence time	3, 10, 20, 30 ms
Volume flow	0.00033 m^3
Pressure	20 bar
Φ	0.5, 1

Table 5: Conditions set in the PFR for the different simulations.

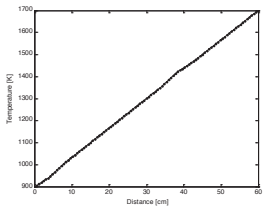

Figure 21: Temperature profile used in the simulations with the PFR.

The conditions in the PFR during the simulations are shown in table 5. Also in the PFR the conditions fit those in the AEV burner. Note that the residence time 1 ms is not simulated in the PFR due to convergence difficulties.

As in the PSR the gas temperature is fixed. However in the PFR the temperature is changed according to the temperature profile shown in figure 21. The "bumps" on the curve is where the temperature has been slightly altered to help the convergence in the simulations.

For the PFR the ignition and burnout temperature is defined in the same way as for the PSR.

9.3.1 Comparison of gas A, B and C

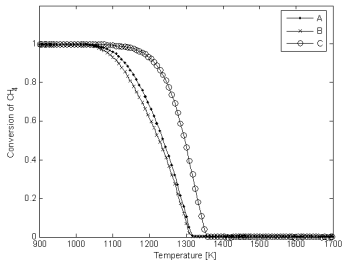

Figure 22: Combustion of gas A, B and C for Φ=1 and τ=3 ms and 20 bar.

Mechanism IV Figure 22 shows simulations from a PFR with the residence time 3 ms and Φ=1. Comparing figure 17 and figure 22 the curve for the PFR has a more abrupt burnout and that the rate of combustion, when started, is higher for the PFR.

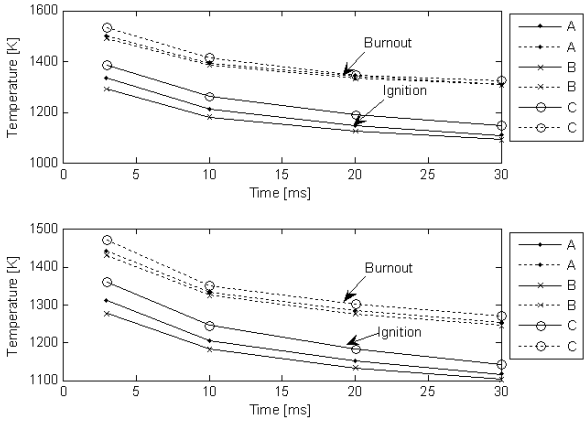

Figure 23: Combustion of gas A, B and C for Φ=1 (above) and Φ=0.5 (below). Ignition and burnout temperatures are represented with dotted lines and lines respectively and the different gases are represented with different patterns.

Figure 23 shows the ignition and burnout temperatures versus the residence times when combusting gas A, B and C. The ignition temperature at 3 ms varies, when Φ=1, between 1293 K, gas B and 1386 K for gas C. When Φ=0.5 the temperature spread is smaller from 1277, for gas C to 1357 for gas B. The lower ignition temperatures when Φ=0.5 is explained by the decreased methane fraction discussed earlier.

Mechanism I The results from simulations with mechanism I are found in figure 24.

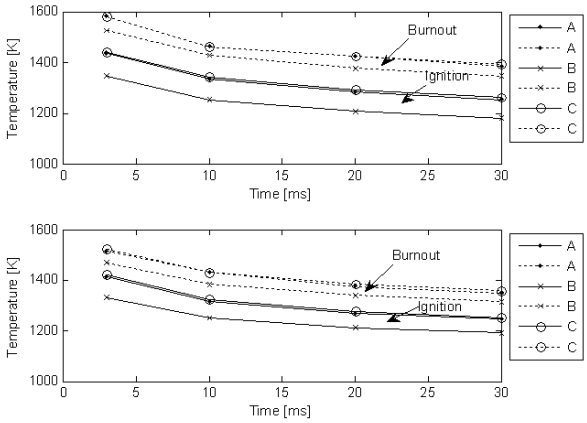

Figure 24: Ignition and burnout temperatures as function of residence time when combusting gas A, B and C at Φ=1 (above) and Φ=0.5 (below).

Comparing the simulations from mechanism I and IV the ignition and burnout temperatures has increased with mechanism I. The gas with the most change in ignition temperature due to mechanism change is gas A. As discussed earlier the increase in ignition temperature for gas A is probably due to the change in composition when recalculating the hydrocarbons from mechanism IV to I.

9.3.2 Conclusion

The PSR simulations with mechanism IV show that the gas with the highest reaction temperature is gas C. Mechanism I shows the highest ignition temperature for both gas A and C but as discussed earlier the high ignition temperature for gas A could be a result of the gas recalculation. Due to this it is reasonable to believe that the gas with the highest ignition temperature is gas C which then has an 80 degrees higher ignition temperature according to mechanism IV. This can be explained by the high methane fraction in the gas also discussed earlier.

In the PFR the results are consistent with those in the PSR. The gas differing most in ignition temperature for the two reactors is gas C. In table 6 the ignition temperatures for both the reactors with the conditions Φ=1 and Φ=0.5 is shown. The table shows, as mentioned above, that the ignition temperature for gas C is the highest for both Φ=1 and Φ=0.5.

Gas	PSR Φ=1	PFR Φ=1	PSR Φ=0.5	PFR Φ=0.5
A	1040 K	1333 K	1040 K	1309 K
B	1030 K	1293 K	1030 K	1277 K
C	1070 K	1386 K	1050 K	1357 K

Table 6: Ignition temperatures for the PSR and PFR. Biggest differance between the reactors is achved with gas C and Φ=0.5.

The results from the simulations in both reactors all indicate that the temperatures increase with increasing Φ and that the gas with the highest ignition temperature is gas C. Whether the difference in ignition temperature is due to the high methane fraction or the low fraction of higher hydrocarbons is unclear. The ignition and burnout temperatures however differ between the reactors. The temperatures and combustion rate are higher in the PFR than in the PSR due to that no back mixing occurs in the PFR which in the PSR causes the heated combustion gases to pre-heat the non combusted gas which eases the ignition.

Since the gases in the combustion chamber are recirculated it is possible that the most accurate reactor to use is the PSR.

10 Solving the energy equation

Solving the energy equation, (13), with the term Q_{loss}= 0 gives the adiabatic flame temperature. The flame temperature depends on start temperature, pressure and the composition of the fuel gas. The adiabatic flame temperature gives the highest possible temperature for the gas at the given pressure and inlet temperature. For the simulations the inlet temperature was set to 298.15 K, room temperature, the pressure to 20 bar and the composition of the gases set as in table 3.

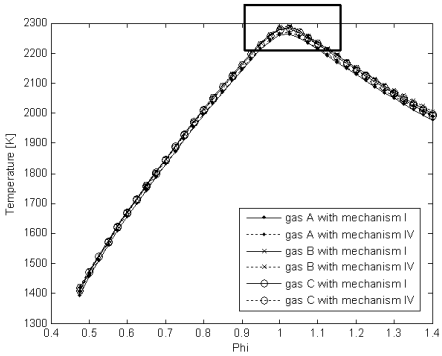

Figure 25: Adiabatic flame temperature for gas A, B and C with mechanism I and IV. The square shows the enlargement made into figure 26

Figure 26 is an enlargement of figure 25. The figures show the adiabatic flame temperature as a function of Φ. The temperature peaks at the same Φ for all three gases, the maximal temperature however differs both between the gases and the mechanisms. The difference in maximal temperature between mechanism I and IV only exists for gas A and B with 5 and 7 degrees respectively. The gas with the highest adiabatic temperature is gas B followed by gas C and A. The difference in temperature between the gases is between 15 and 30 degrees.

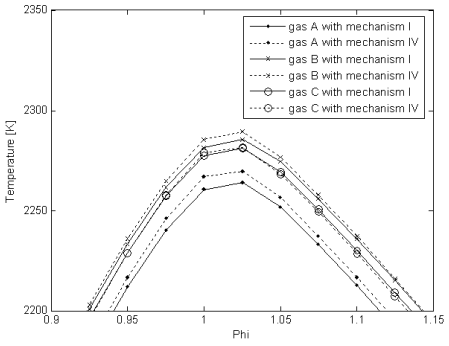

Figure 26: Adiabatic flame temperature. Enlargement from figure 25

10.1 Conclusion

The difference in flame temperature is mainly due to the difference in nitrogen fraction in the different gases. Simulations made with a mixture of methane and nitrogen where the fraction of nitrogen varied shows that the fraction of nitrogen influences the adiabatic flame temperature, see Appendix B. The ignition and burnout temperature however does not change with the varying nitrogen fraction. The reason for the change in adiabatic flame temperature although the nitrogen is not chemically bound is that the nitrogen dilutes the methane and thereby increases the species that are to be heated. At the same time the fraction of the reacting species contributing to the heat is decreased. The difference in flame temperature results in that for gas A to have the same flame temperature as gas B gas A needs to be preheated 30 degrees.

11 Simulation of NOx − formation

The species NO, NO_2 and N_2O are, among others, included in the expression nitrous oxides, NO_X. The formation of NO_X can be parted into the three categories, fuel, thermal and prompt NO_X. The fuel NO_X is included in the fuel, thermal NO_X is formed at temperatures above 1500 K while the prompt NO_X is formed directly when the nitrogen reacts with the hydrocarbon radicals in the fuel.[1]

A NO_X mechanism from reference [8] was included in mechanism I and IV. Since the intermediate species differ between the mechanisms, an emission comparison between the mechanisms was made. The comparison verified that no difference in emissions between the two mechanisms existed. Hence the simulations were only made with mechanism IV. In the simulations NO_X is the sum of NO, NO_2 and N_2O. For the simulations a PSR was used.

Φ	$0.45 - 1.45$
τ	3, 10, 20, 30 ms
p	20 bar
Q_{loss}	0 kJ/s
T_{in}	298.15 K

Table 7: Conditions used for simulations when solving the energy equation with varying Φ.

The conditions used when solving the energy equation are tabulated in table 7. Solving the energy equation for different residence times gives the NO_X emissions as a function of Φ. The NO_X emissions reach a maximum at Φ_{max}=0.95 independent of residence time.

Figure 27 shows the adiabatic flame temperature and the NO_X emissions when combusting gas A at various residence times. The figure shows that the emissions decrease with decreasing residence time. If Φ is increased to 1 from 0.95 the NO_X emissions are decreased 18 % and when decreased with 0.05 the emissions decrease 30%.

In the simulations with varying temperature Φ was set to 0.95. The temperature varied from 1700 to the adiabatic flame temperature. The conditions used in the simulations with fixed Φ are seen in Table 8. The emissions were recalculated to levels with 15 percent O_2.

Φ	0.95
τ	5, 10, 20, 30 ms
p	20 bar
T	$1700 - T_{ad}K$

Table 8: Conditions for simulations with fixed gas temperature.

In figure 28, the emissions from gas A at Φ=0.95 and different temperatures below the adiabatic are seen. It is desired to reach a maximum NO_X level of 15 ppm from the AEV burner and, in the future possibly 9 ppm. This gives for

the residence time 5 ms a maximum temperature of 1972 K and 1905 K for 15 and 9 ppm respectively.

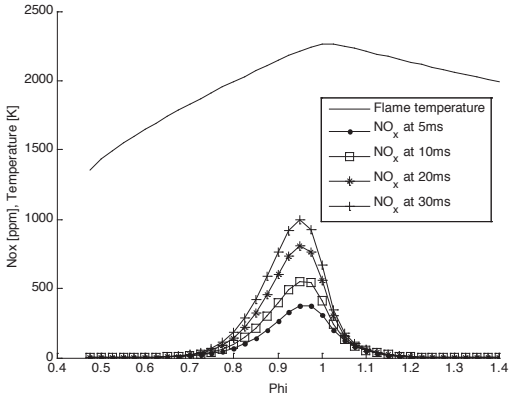

Figure 27: Adiabatic flame temperature and NOx at varying Φ for gas A. The different dots represent different residence times.

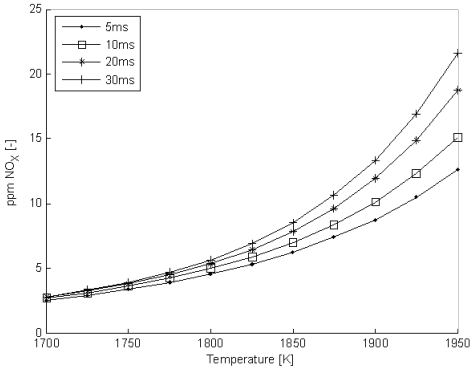

Gas	NO_X at Φ=0.95 and τ=5 ms	Temperature for 15 ppm NO_X at Φ=0.95 and τ=5 ms	Temperature for 9 ppm NO_X at Φ=0.95 and τ=5 ms
A	113 ppm	1972 K	1905 K
B	132 ppm	1965 K	1892 K
C	130 ppm	1980 K	1914 K

The emissions from all three gases are tabulated in table 9. A comparison between the gases maximum emissions gives that gas B has the highest emissions explained by the 30 degrees higher adiabatic flame temperature than gas A has.

With the requirement of a maximum NO_X level at 15 and 9 ppm it is also gas B that has the lowest allowed temperature to pass the requirement.

11.1 Conclusion

The maximal emissions for all three gases are found at Φ=0.95, to obtain low NO_X emissions this area should therefore be avoided. If Φ is increased or decreased 0.05 the NO_X emissions rapidly decreases. The gas with the highest emissions is gas B which also has the highest adiabatic flame temperature. Thermal NO_X will form at high temperatures and is the probable reason for the higher emissions. With the restrictions 15 and 9 ppm of NO_X the allowed temperatures for the gas is the lowest for gas B.

12 Laminar flame speed

The flame speed depends both on the inlet temperature and the pressure. The speed increases with the temperature and decreases with increasing pressure. The flame speed also varies with Φ in the same way as the adiabatic flame temperature. If the flame speed is greater than the velocity of the gas flashback will occur, if the flame speed instead is less than the gas velocity the consequence will be a burnout.

The laminar flame speed was determined through the Premixed Laminar Flame-Speed model. The conditions set for the simulations are seen in table 10. The initial temperature profile for the simulations is seen in figure 29(a). The profile is received from another simulation and is, as mentioned earlier, only an initial temperature profile. However the closer the initial profile is to the actual temperature profile, the shorter the simulation time is.

Φ	1
p	20 bar
T	see figure 29(a)

Table 10: Conditions set for simulations in the premixed laminar flame speed model.

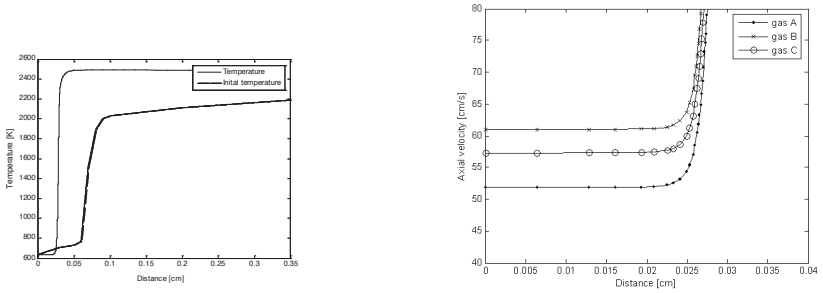

(a) (b)

Figure 29: a) Temperature profile for flame speed calculations. b) Laminar flame speeds for gas A, B and C.

In figure 29(b) the axial velocity as a function of distance is shown. The velocity is almost constant until the distance 0.025 cm where a sudden increase takes place. This increase is due to the fuel that is combusting and then expanding, increasing the velocity. The laminar flame speed is the velocity until the sudden increase in velocity occurs at 0.025 cm.

Figure 29(b) shows that the laminar flame speed for gas A, 52 cm/s, is about 15% lower than gas B, 61 cm/s, and 9% lower than C, 57 cm/s.

12.1 Conclusion

The laminar flame speed differs between the gases with up to 15%. The turbulent flame speeds would also be relevant since flow in the AEV mainly is turbulent.

13 Conclusion

Summing up the conclusions from the different chapters and comparing the results from the different types of simulations gives a comprehensive picture of the study.

Experimental data would have been preferable to use for validating the accuracy of the chemical mechanisms, but unfortunately no data consistent with the case of our interest was found. Instead when determining which mechanism to use in the simulations mechanism IV was used as a reference when comparing the other mechanisms. The study shows that the mechanisms most similar are mechanism III and IV, mechanism III had however convergence difficulties and mechanism I was instead chosen.

The simulations with the PSR and PFR with mechanisms I and IV show the same tendencies. The ignition temperature decreases with decreased methane fraction due to both a change in Φ and the gas composition, which in turn depends on the consumption rate of radicals by the methane. The highest ignition temperatures were found for the PFR since no back mixing occurs. In reality back mixing will occur due to recirculation and the PSR may therefore be the more suitable reactor to use. The largest difference in ignition temperature between the gases (80 K) was found in the PSR with mechanism IV between gas A and C.

The difference in adiabatic flame temperature is mainly due to the difference in nitrogen fraction between the gases. Gas A, with the highest fraction of N_2, has the lowest adiabatic flame temperature.

The adiabatic flame temperature also influences the NO_X emissions. Is was seen that the gas with the lowest adiabatic flame temperature, gas A, also has the lowest NO_X emissions. For all the gases the highest NO_X emissions were obtained at Φ=0.95. If Φ changes 0.05 from this point the emissions rapidly decreases, hence if low NO_X emissions is a priority the stoichiometry around 0.95 should be avoided. Also seen in the simulations is that the gas with lowest ignition temperature and the highest adiabatic flame temperature, gas B, has the highest emissions of NO_X.

The laminar flame speed differs at the most 15% between the gases. Seen in the simulations is that the gas with the highest adiabatic flame temperature has the highest laminar flame speed.

14 Discussion

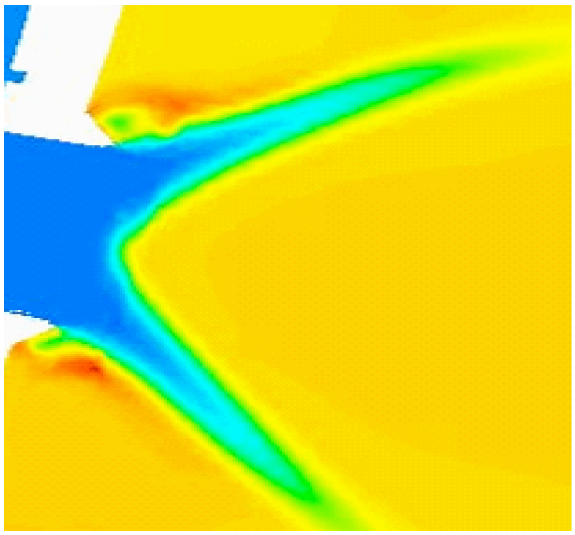

Figure 30: Enlargment of figure 9

The importance of the conclusions from the different simulations applied to the AEV burner discussed below.

The 80 degrees difference in ignition temperature is when applied to figure 30 not a noticeable difference. The flame will be slightly thicker and the flame will be placed slightly higher upstream with the lower ignition temperature. It is possible that the ignition temperature can make a difference if the two ignition temperatures are placed on different sides of the stagnation point. Whether the higher ignition temperature is due to the high methane fraction or the low fraction of higher hydrocarbons is not clear. Probably the combination of high methane fraction and a low fraction of higher hydrocarbons as a combination increases the ignition temperature.

If the temperatures were lower but with the same difference the influence from the temperature difference on the flame would have been bigger. However at these temperatures the conclusion is that the difference will have negligible influence on the flame properties, i.e. the difference in ignition temperature does not influence the combustion at the existing temperatures.

The adiabatic flame temperature only differ 30 degrees but affects the burner more. The 30 degree difference can be compared with a difference in Φ from 0.50 to 0.5135 which in some of the gas turbines can be achieved by bypassing a part of the air. This influences the combustion much more than the 80 degrees difference in ignition temperature. From experience it is known that an increase in adiabatic flame temperature with 20 K increases the NO_X emissions with 2 ppm. With restrictions at 20 ppm this means 10%. For the 30 K difference between the gases this means approximately 3 ppm.

In figure 30 the temperatures that reach high enough for NO_X emissions above the level 15 ppm to be formed are dark red. In the figure Φ equals 0.5 while the simulations are made with Φ=0.95. For the emissions to reach 15 ppm

the temperatures need to be even higher, which does not exist in the figure. The CFD simulation assumes that the fuel and air are perfectly blended which in reality is not the case. There are probably so called hotspots in the flame due to poor mixing, where the temperature will reach levels necessary for 15 ppm NO_X to be formed. The difference in emissions between the gases is however negligible and furthermore the assumptions made in the different calculation models results in that the accuracy needed to predict NO_X is, by far, out of range.

The difference in laminar flame speed is difficult to apply on the turbulent conditions. Probably the difference will not change the turbulent flame speeds in a significant way.

The overall conclusion is that the composition of the natural gas does not influence the performance of the AEV burner noticeably.

15 References

[1] Turns, S.R., An introduction to Combustion, 1993
[2] Andersson, S., Förbränningsteknik, 1996
[3] Chomiak, J., Combustion: A study in theory, fact and application, 1990
[4] Herman, Fredrik. "Investigation of Emission Characteristics for Diluted Flames and Renewable Fuels in Gas Turbine Combustors", Diss. 2005, Lund University
[5] Kee, R. J. et al, Chemkin 4.0 Theory manual, 2004
[6] Kanury, A. M., Introduction to combustion phenomina, 1975
[7] Gas analysis from AGA gas AB, sample number 04.0271, 05.0087, 04.0038
[8] Glarborg, P. et al. (2004), "Ammonia chemistry below 1400K under fuel rich conditions in a flow reactor", in Combustion and flame, vol. 136, pp 501-518
[9] Smith, G.P. et al., Gas Research Institute,1999
[10] Heyberger, R et al., Departement de chimie physique des reactions, (2002)
[11] Curran, H. J., Gaffuri, P., Pitz, W. J., and Westbrook, C. K.,"A Comprehensive Modeling Study of n-Heptane Oxidation", in Combustion and Flame, vol 114, pp 149-177, 1998

16 Acknowledgements

This master thesis work started in August 2005 at Siemens Industrial Turbomachinery in Finspång. Many thank's to Jenny Larfeldt for the exellent tutoring, Karl-Uno Andersson for all the help with the chemistry and Chemkin and Johan Revstedt for helpfull discussions.

17 Appendices

17.1 Appendix A

17.1.1 Species included in mechanism I

CO	CO2	NO	HCN	H	O
OH	HO2	O2	H2	H2O2	H2O
CH2O	HCO	CH4	CH3	CH2	CH2(S)
CH	C	CH3OH	CH3O	CH2OH	C2H6
C2H5	C2H4	C2H3	C2H2	C2H	C2
CH3HCO	CH2HCO	CH3CO	C2H2OH	OCHCHO	CH2CO
HCCOH	HCCO	C2O	C2H5CHO	C2H5CO	NO2
NO3	HNO	HONO	H2NO	NH3	NH2
NH	N	N2H2	NNH	N2O	CN
NCO	HNCO	HOCN	HCNO	C2N2	NCN
CH3CN	CH2CN	H2CN	AR	N2	N2H4
N2H3	H2NN	HON	HNOH	HNNO	NH2OH
NH2NO					

17.1.2 Species included in mechanism IV

h	h2	o	o2	oh	co2
h2o	n2	hco	h2o2	ho2	c2h6
ch3	co	ch4	c2h4	ch3o	c2h5
ch2	ch	c2h	c2h2	ch2o	c2h3
ch2oh	ic4h10	ch3o2h	c2h5o2h	ch2cho	ic5ketda
c3h4-p	cc5h11	c2h5o2	c2h3o1-2	o2c4h8oh-2	ic5ketdb
c3h8	dc5h11	ch3o2	ch3co2	o2c4h8oh-1	c4h8ooh1-3o2
c3h6	ac5h10	c2h5o	c2h4o1-2	c4h8oh-2	ic4h8ooh-to2
c4h6	bc5h10	ch3coch2o2	c2h4o2h	c4h8oh-1	ic4h8ooh-io2
ic3h7	cc5h10	ch3coch2o2h	o2c2h4oh	c4h7o	tc4h8ooh-io2
nc3h7	ic5h12	cc5h10ooh-b	ch3co3	ic4h7o	c4h8ooh2-4o2
c4h8-1	ac5h11	dc5h10ooh-a	ch3co3h	io2c4h8oh	c4h8ooh2-3o2
ic3h7o2	bc5h11	dc5h10ooh-b	c2h3co	ic4h8oh	c4h8ooh2-1o2
nc3h7o2	c4h8-2	dc5h10ooh-c	c2h3cho	ic3h5cho	c4h8ooh1-4o2
ic3h7o2h	c4h7	neoc5h10ooh	c2h5oh	tc3h6ocho	bc5h10ooh-a
nc3h7o2h	c4h10	c5h10ooh1-2	ch3cho	tc3h6cho	bc5h10ooh-c
sc4h9o2	c2h5co	c5h10ooh3-2	ch3oh	c3h6ooh2-1	bc5h10ooh-d
pc4h9o2	c2h5cho	ac5h10ooh-a	pc2h4oh	ic3h7cho	c6h12ooh3-1o2
ic5ketdc	c5h10-1	c5h10ooh2-3	nc5h12	c3h6ooh1-2	c7h14ooh2-5o2
dc5h11o	ch3co	c5h10ooh2-1	ic4h8o2h-t	c3h6ooh1-3	cc5h10ooh-d
ic4h9o2	sc2h4oh	c3h6ooh1-3o2	c5h11o2-2	ac5h11o2	ac5h10ooh-c
c4h8o1-3	6c5h9	c3h6ooh1-2o2	a-ac5h10o	bc5h11o2	cc5h10ooh-do2

Continuation of species included in Mechanism IV

ic5ketcd	ch2co	c5h10ooh1-3	c-dc5h10o	cc5h11o2	bc5h10ooh-do2
ic4h7ooh	pc4h9o	c2h5coc2h4p	dc5h11o2	dc5h11o2h	cc5h10ooh-ao2
c4h8o1-2	sc4h9o	c5h10ooh1-5	tc4h8o2h-i	ac5h11o	cc5h10ooh-bo2
c4h8o1-4	ic4h9o	c5h10ooh2-5	b-dc5h10o	cc5h11o	c4h8ooh1-2o2
nc4ket21	tc4h9o	pc2h4coc2h3	b-cc5h10o	c5h11o-2	ac5h10ooh-b
nc4ket12	c4h10o	neoc5h11o2h	a-dc5h10o	ch3coch2o	c5h10ooh3-1
nc4ket13	ic5h9	ac3h5chcho	a-cc5h10o	c4h8ooh1-3	dc5h10ooh-ao2
nc4ket14	c3h4-a	ch2ch2coch3	c5h11o2-3	c2h3-ch2o	dc5h10ooh-bo2
neoc5ket	cc4h8o	ic3h6chcoch3	nc5ket21	c4h8ooh1-4	dc5h10ooh-co2
nc5ket32	hcco	c3h6coc2h5-1	nc5ket23	o2c2h4o2h	ac5h10ooh-bo2
nc4ket23	c3ket13	c5h10ooh2-4	nc5ket25	ch2o2hcho	c5h10ooh2-4o2
c3h6o1-2	bc5h11o	ch3choococh3	nc5ket24	c4h8ooh2-1	c5h10ooh1-3o2
ic5ketab	c3h5o	c2h5coc2h4s	c2h3coch3	cc5h11o2h	c5h10ooh2-1o2
nc5ket12	c3ket21	tc3h6coc2h3	c2h5coch3	c5h11o2h-1	c5h10ooh1-2o2
ic5ketac	c3ket12	c5h10ooh1-4	c5h11o2-1	c4h8ooh2-3	c3h6ooh2-1o2
nc5ket15	ic4ketii	c3h6coch3-2	ic4h8o2h-i	c5h11o2h-2	bc5h10ooh-ao2
nc5ket13	c3h5-a	c3h6coch3-3	c5h10o1-4	c5h11o2h-3	o2neoc5h10ooh
nc5ket14	ic5ketaa	c3h6coc2h5-3	c5h10o2-4	neo-c5h10o	c5h10ooh3-2o2
ic3h5co	c3h5-s	nc3h7coc2h4p	c5h10o2-3	bc5h11o2h	c5h10ooh3-1o2
tc4h8cho	c3h5-t	nc3h7coc2h4s	c5h10o1-5	neoc5h11o2	c5h10ooh2-5o2
c4h8o2-3	c3h3	nc3h7coc2h5	c5h10o1-3	neoc5h11o	ac5h10ooh-ao2
nc5ket31	c3h2	ic3h6coc2h5	ic5ketad	nc4ket24	c5h10ooh1-4o2
ic3h6cho	ch3chco	c3h6coc2h5-2	ic3h6chco	ic3h6chcho	bc5h10ooh-co2
ic5ketcb	hco3h	c6h12ooh1-2	c5h10o1-2	o2c4h8cho	c5h10ooh1-5o2
nc3h7cho	hco3	c6h12ooh1-3	c3h6cho-1	c6h13o2-2	ch3choohcoch3
nc4h9cho	hco2	c6h12ooh3-6	c6h12o3-4	ch2cch2oh	c5h10ooh2-3o2
ac3h5cho	ic4ketit	c6h12ooh1-4	ch3chcho	tc3h6o2hco	ac5h10ooh-co2
nc6ket13	ic3h7co	c6h12ooh2-5	ch2ch2cho	tc3h6ohcho	ac5h10ooh-do2
ic3h6cho	ic3h5oh	c6h12ooh3-4	c3h6cho-3	c2h5coc2h5	ch2choohcoch3
nc6ket14	tc3h6oh	c6h12ooh3-5	c3h6cho-2	ch3chocho	ac3h5chcoch3
nc6ket23	c3h5oh	c6h12ooh3-2	c2h5chco	tc3h6o2cho	ic3h6chcoch2
c6h13o-1	nc6h14	ic3h6coc2h3	c6h12o1-3	ic3h5coch36	c7h14ooh2-6o2
nc6ket21	c6h13-1	c6h12ooh2-6	sc3h5cho	c2h5coc2h3	c7h14ooh3-1o2
c6h13o-3	ic5ketca	ic3h7coc2h5	c6h13o2-3	o2hc4h8co	c3h6coch3-1
nc6ket24	nc3h7co	c7h14ooh1-5	c4h8cho-3	o2hc4h7cho	c7h14ooh2-3o2
nc6ket25	sc3h5co	c6h12ooh1-5	c4h8cho-1	ic3h5coch2	c7h14ooh2-4o2
nc6ket15	c6h13-3	c7h14ooh3-6	c6h12o1-2	ic3h6coch3	ic3h5coc2h4p
nc6ket26	nc4h9co	c7h14ooh3-7	c4h8cho-4	ic3h7coch3	ic3h5coc2h4s
nc6ket32	c6h12-1	c7h14ooh4-1	c6h12o1-4	ic3h7coch2	c6h12ooh3-5o2
c6h13o-2	c6h13-2	c7h14ooh4-2	c6h12o2-3	sc3h5coch2	c6h12ooh1-3o2
nc6ket36	c7h14-1	c7h14ooh4-3	c6h12o2-4	c6h12o1-5	c6h12ooh3-1
nc6ket35	c7h15-1	c4h6cho1-44	c4h8cho-2	c6h13o2h-1	c6h12ooh3-2o2

Continuation of species included in Mechanism IV

nc6ket12	ac3h5co	c6h12ooh2-3	c6h13o2-1	tc3h6coch3	c6h12ooh1-5o2
c7h15o-3	c7h14-2	c4h8coch3-2	nc6ket31	c6h13o2h-2	c6h12ooh2-1o2
c7h15o-4	c6h11	c4h8coch3-3	c2h3chcho	ac3h4coch3	c6h12ooh1-4o2
nc7ket12	c6h12-3	c4h8coch3-4	c7h15o2-2	c7h15o2h-3	c6h12ooh1-2o2
c7h15o-1	c6h12-2	c7h14ooh2-5	c7h15o2-3	ch3chcoch3	c6h12ooh2-3o2
nc7ket13	c7h15-2	c7h14ooh2-4	c7h15o-2	c7h15o2h-1	c6h12ooh2-4o2
nc7ket14	c7h15-3	ic3h7coc2h3	c7h15o2-4	c7h15o2h-2	c6h12ooh2-5o2
nc7ket15	c7h13	c6h12ooh2-4	c6h12o2-5	c6h13o2h-3	c6h12ooh2-6o2
nc7ket21	c7h14-3	c7h14ooh2-1	c7h14o3-5	c7h15o2h-4	ic3h7coc2h4s
nc7ket23	nc7h16	tc3h6coc2h5	c7h15o2-1	nc4h9coch3	c6h12ooh3-6o2
nc7ket24	c7h15-4	c6h12ooh2-1	c7h14o1-3	c5h10cho-2	ic3h7coc2h4p
nc7ket25	ic3h7o	c7h14ooh3-4	c7h14o1-4	nc4h9coch2	c6h12ooh3-4o2
nc7ket35	nc3h7o	ic3h5o2hcho	c7h14o1-2	c5h10cho-3	c7h14ooh2-1o2
nc7ket26	ar	c4h6cho1-43	c7h14o1-5	c5h10cho-4	c7h14ooh1-2o2
nc7ket34	he	c7h14ooh3-5	c7h14o2-3	c5h10cho-5	c7h14ooh1-3o2
nc7ket31	ic4h8	c7h14ooh1-2	c7h14o2-4	c4h7cho1-4	c7h14ooh1-4o2
nc7ket32	ic4h7	c7h14ooh2-6	c7h14o2-6	nc3h7coch2	c7h14ooh1-5o2
nc7ket36	pc4h9	c4h8coch3-1	c7h14o3-4	nc5h11cho	c7h14ooh3-2o2
nc7ket37	ic4h9	c7h14ooh1-4	c4h7co1-4	c5h10cho-1	c7h14ooh3-4o2
nc7ket42	tc4h9	c7h14ooh3-1	c7h14o2-5	nc3h7coch3	c7h14ooh3-5o2
nc7ket43	sc4h9	c7h14ooh3-2	c2h5coch2	ac5h11o2h	c7h14ooh3-6o2
nc7ket41	c5h11-3	c7h14ooh3-4	nc5h11co	c4h8ooh1-2	c7h14ooh3-7o2
nc6ket34	c5h11-2	c7h14ooh3-5	sc4h9o2h	c4h8ooh2-4	c7h14ooh4-1o2
ch3coch3	c5h11-1	sc2h4coc2h3	c5h11o-1	a-bc5h10o	c7h14ooh4-2o2
c5h11o-3	c5h10-2	c7h14ooh2-3	tc4h9o2h	ic4h9o2h	c7h14ooh4-3o2
pc4h9o2h	tc4h9o2	ch3coch2	neoc5h11	neoc5h12	c7h14ooh1-3

17.2 Appendix B

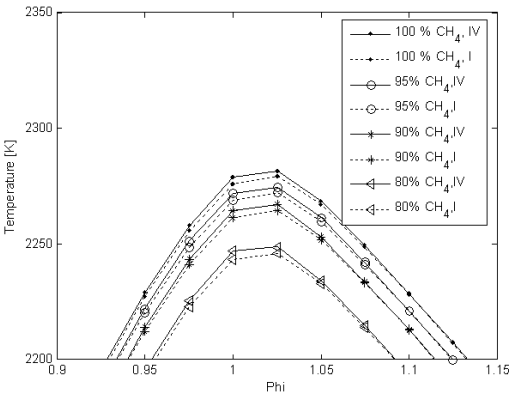

Figure 31: Adiabatic flame temperature for various fractions of N2 and different mechanisms.

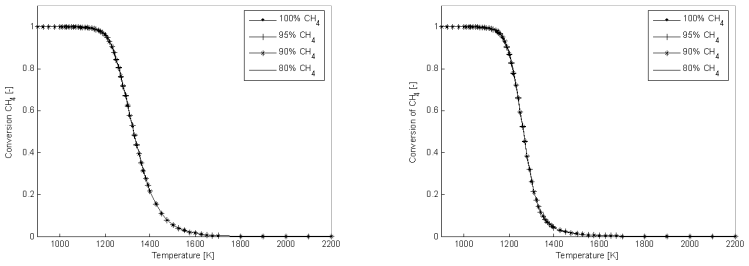

(a) (b)

Figure 32: Influence of N2 when combusting methane at 1 ms, 20 bar and with a) Φ=1 and b) Φ=0.5.

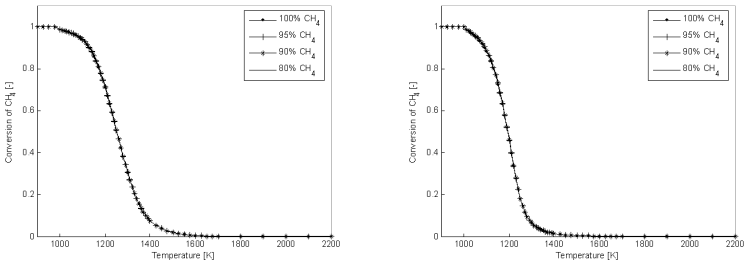

(a) (b)

Figure 33: Influence of N2 when combusting methane at 3 ms, 20 bar and with a) Φ=1 and b) Φ=0.5.

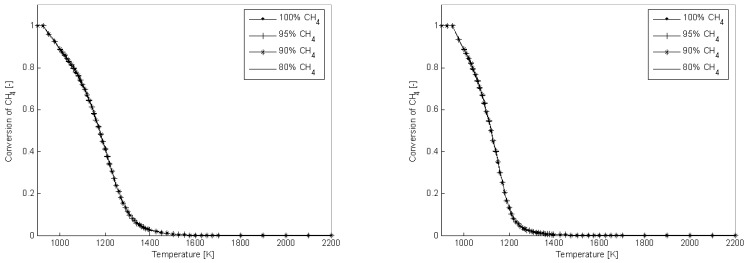

(a) (b)

Figure 34: Influence of N2 when combusting methane at 10 ms, 20 bar and with a) Φ=1 and b) Φ=0.5.

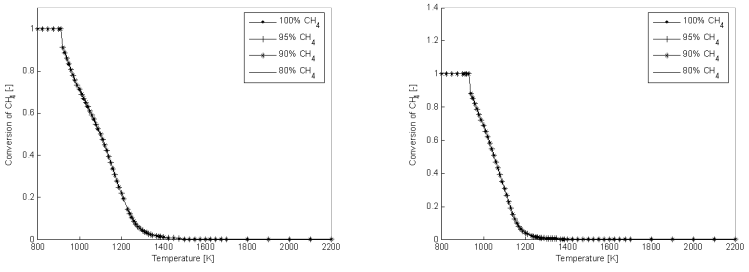

(a) (b)

Figure 35: Influence of N2 when combusting CH4 at 30 ms, 20 bar and with a) Φ=1 and b) Φ=0.5.